Ionic cocrystals of etiracetam and levetiracetam: the importance of chirality for ionic cocrystals

Lixing Song,[†] Oleksii Shemchuk,[‡] Koen Robeyns,[†] Dario Braga,[‡] Fabrizia Grepioni,[‡*] Tom Leyssens[†*]

†Institute of Condensed Matter and Nanosciences, Université catholique de Louvain, Place Louis Pasteur 1, 1348 Louvain-la-Neuve, Belgium;

‡Dipartimento di Chimica "Giacomo Ciamician", Università di Bologna, Via Selmi 2, 40126 Bologna, Italy

ABSTRACT: A striking variety of anhydrous and hydrated ionic cocrystals (ICCs) of the enantiopure anti-epileptic drug (AED) levetiracetam and of its racemic intermediate etiracetam with the pharmaceutically acceptable salts $CaCl_2$ and $MgCl_2$ was synthesized and structurally characterized. The difference in the interaction of enantiopure and racemic compounds of interest with the inorganic salts was investigated. Variable temperature X-ray powder diffraction (VT XRPD) and calorimetric analyses (TGA and DSC) of all obtained ICCs showed a significant improvement in thermal stability with respect to pure racetams.

INTRODUCTION

Epilepsy is a prevailing chronic neurological disorder or a group of disorders characterized by unprompted seizures which tend to recur.[1] More than 50 million people worldwide are affected by this condition.[2] Levetiracetam ((S)-2-(2-oxopyrrolidin-1-yl)butanamide, Fig. 1) is the active pharmaceutical ingredient (API) of KEPPRA®, an anti-epileptic drug (AED) commercialized by UCB Pharma. Levetiracetam is one of the most recent AEDs that has been approved by Food and Drug Administration in 1999.[3]

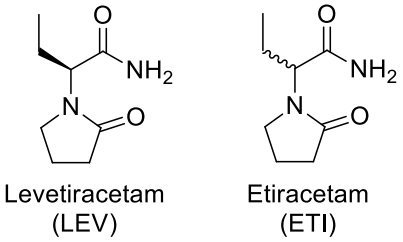

Fig. 1. The chemical structure of Levetiracetam and Etiracetam

Etiracetam is encountered as a racemic intermediate in the synthesis of levetiracetam. The racemic compound contains, besides the active S-enantiomer (levetiracetam) of pharmaceutical interest, R-etiracetam, which does not exert the desired biological properties.[4]

Ionic cocrystals[5-10] (ICCs) are multicomponent crystalline solid forms composed of neutral organic molecules and salts in a defined stoichiometric ratio. Due to their potentially more effective capacity to alter in a desired way the physicochemical properties of interest (e.g. solubility, intrinsic dissolution rate, bioavailability, morphology, hygroscopicity and thermal stability), ICCs are increasingly attracting the attention of the scientific community.[6, 11-18] Cocrystals in general, and ICCs in particular, are of enormous interest for the pharmaceutical industry, since they can provide an alternative route to new pharmaceutical formulations compared to conventional salts. Particularly, the formation of cocrystals can be of use if the API of interest has no ionizable moieties, such as the compounds discussed in this work. In the absence of ionizable groups and consequent salt formation, molecular cohesion is usually enhanced in molecular cocrystals by hydrogen and/or halogen bonds and π-π stacking, whereas coulombic forces (ion-ion and ion-dipole) are also at work and dominant in ICCs. Besides their possible effect on the physicochemical properties of the API,[19] cocrystals have potential implications on intellectual property issues.[20]

Cocrystallization of chiral molecules has been extensively studied by our groups, and has proven to be a useful approach for the chiral resolution of racemic mixtures. We showed that the application of (S)-mandelic acid as a coformer allows to resolve a racemic solution of etiracetam,[21-22] via selective formation of cocrystals with the S-enantiomer – the enantiomer which possesses anti-epileptic activity. Although this approach resembles the conventional method of chiral resolution by salt formation, cocrystals between the coformer (S)-mandelic acid and the opposite enantiomer (R-etiracetam with S-mandelic acid) could not be obtained, once more highlighting the differences of cocrystals with respect to salts.

Quite unexpectedly, ICCs formation has been found to offer an additional tool for chiral resolution, as recently discovered for the ionic cocrystals of alkali and alkaline earth halides with the amino acids DL-histidine[23-24] and DL-proline.[25] The use of lithium halides results in a marked preference for Li^+ to selectively link the amino acids of only

one chirality, with formation either of conglomerates or of racemic crystals constituted of homochiral chains.[22-23]

Recently we showed for the first time that, in the cocrystallization of levetiracetam and etiracetam with $ZnCl_2$, the stoichiometry ratio could be used to reversibly switch between a racemic compound and a conglomerate.[26]

In this paper we take the ICC approach further, and cocrystallize both enantiopure and racemic etiracetam with inorganic salts accepted by the pharmacopoeia, i.e. $CaCl_2$ and $MgCl_2$. Taking into account the relatively low melting points of the pure racetams (116 °C and 119 °C for the enantiopure and the racemic compounds, respectively),[27] it was expected that, upon cocrystallization with the inorganic salts, thermal stability enhancement could be achieved. This assumption was supported by our previous study[28] of ICCs of brivaracetam and seletracetam with calcium and magnesium chlorides. In the present case we also wanted to explore the behavior of racemic *vs*. enantiopure pharmaceuticals in ICCs of alkaline earth with respect to that observed with alkali metal salts, with a particular focus on the thermal stability of the compounds in the solid state.

EXPERIMENTAL SECTION

Materials. S-2-(2-oxopyrrolidin-1-yl)butanamide (levetiracetam) was purchased from Xiamen Top Health Biochem Tech. Co., Ltd. (RS)-2-(2-oxopyrrolidin-1-yl)butanamide (etiracetam) was prepared by racemization of S-2-(2-oxopyrrolidin-1-yl)butanamide. 10 g of S-2-(2-oxopyrrolidin-1-yl)butanamide together with a catalytic amount (0.05 eq.) of MeONa were added to 10 mL of methanol. The solution was kept under reflux and continuous stirring for 24 h, then cooled to room temperature. The compound crystallizes spontaneously. After filtration, the compound was washed twice with methanol and used as such. All other reagents were purchased from Sigma and used without purification.

Solution experiments. All samples were prepared by dissolution of the starting materials API:MX_2 (API=LEV or ETI and MX_2= $CaCl_2$ or $MgCl_2$) in 1:1, 2:1 and 4:1 stoichiometric ratios in ethanol, methanol or water; the solution was left to evaporate at room temperature. In some cases single crystals were directly obtained from solution; in other cases the slow evaporation brought about the formation of oils, and single crystals were obtained from these oils, left standing in the air at ambient conditions for 1 to 10 days. The results are shown in Table 1.

Slurry experiments. All slurry experiments were performed by stirring aqueous suspensions of the starting materials in 1:1, 2:1 and 4:1 stoichiometric ratios. The total mass of starting materials was 100 mg. The amount of water was set at 80 µL for the $CaCl_2$ experiments, and at 60 µL for the $MgCl_2$ experiments. The suspensions were seeded with starting materials and corresponding cocrystals and stirred at 25 °C over 48 h to make sure that the system reached thermodynamic equilibrium. Then samples were filtered over sintered glass, followed by XRPD analysis of the solid phases. The results are shown in Table 1.

Liquid assisted grinding (LAG). Powder samples can be obtained mechanochemically through LAG of different stoichiometric mixtures of LEV or ETI and $CaCl_2$ or $MgCl_2$, with the addition of 10 µL of methanol. The sample was ground in a RETSCH Mixer Mill MM 400 for 90 min with a beating frequency of 30 Hz. The results are shown in Table 1. $ETI_4{\cdot}MgCl_2{\cdot}4H_2O$ was obtained by LAG of ETI and $MgCl_2$ (2 to 1) for 60 minutes in a Retsch MM200 ball miller, operated at a frequency of 25 Hz, in the presence of a few drops of methanol.

Hot stage microscopy (HSM). Single crystals of $ETI_2{\cdot}MgCl_2{\cdot}2H_2O$ were obtained using HSM. The measurements were carried out using a Linkam TMS94 device connected to a Linkam LTS350 platinum plate. The powder of $ETI_2{\cdot}MgCl_2{\cdot}6H_2O$ was put in fomblin. The sample was heated up to 110 °C and kept at this temperature for 30 minutes. The sample was then slowly cooled down (5 °C /min) to room temperature and the obtained crystals were analyzed.

Single crystal X-ray diffraction (SCXRD). Data collection was carried out in an Oxford X'Calibur S CCD diffractometer equipped with a graphite monochromator (Mo-Kα radiation, λ = 0.71073 Å) at room temperature and a MAR345 using monochromated MoKα radiation (λ = 0.71073 Å) (Xenocs Fox3D mirror) produced by a Rigaku UltraX18S rotating anode at room temperature. Refinement details are listed in Table 2. All non-hydrogen atoms were refined anisotropically. H_{NH} and part of the H_{OH} atoms were located from difference Fourier maps and refined. H_{CH} and the remaining H_{OH} atoms were added in calculated positions and refined riding on their respective C and O atoms. SHELX-2014[29] was used for all structure solutions and refinements on F^2.

X-ray powder diffraction (XRPD) and variable-temperature X-ray powder diffraction (VT-XRPD). X-ray powder diffraction data were collected with a PANalytical X'Pert Pro and on a Siemens D5000 diffractometer equipped with a Cu X-ray source operating at 40 KV and 40 mA and the secondary monochromator allowing to select the Kα radiation of Cu (λ = 1.5418 Å). A scanning range of 2θ values from 5° to 50° at a scan rate of 0.6° min^{-1} was applied. VT-XRPD diffractograms were collected in the 5-50° 2θ range on a PANalytical X'Pert PRO automated diffractometer, equipped with an X'Celerator detector and an Anton Paar TTK 450 system for measurements at controlled temperature. Data were collected in the open air in Bragg-Brentano geometry, using Cu-Kα radiation without a monochromator. Thermal programs were selected on the basis of TGA results.

Differential scanning calorimetry (DSC). DSC measurements were performed on a TA DSC2500 with Tzero technology calibrated with indium under 50 mL/min continuous nitrogen flow. Samples were prepared in aluminium Tzero pans with punctured hermetic lid. The

temperature profile applied starts at 30 °C and increases up to 220 °C with a rate of 2 °C /min.

Thermogravimetric analysis (TGA). TGA measurements were performed on a Mettler Toledo TGA /SDTA851[e] using an alumina crucible. The heating profile applied starts at 25 ° C and goes up to 300 °C with a rate of 2 °C /min under continuous nitrogen flow of 50.0 mL/min.

RESULTS AND DISCUSSION

The reactivity of both levetiracetam and etiracetam (in the following LEV and ETI, respectively) with calcium and magnesium chlorides was investigated by three different methods, namely liquid assisted grinding (LAG, also called kneading[30]), slurry, and solvent slow evaporation of undersaturated solutions. The latter method inevitably led to the formation of viscous oils, irrespective of the solvent used (water, methanol or ethanol) from which solids precipitated in a period ranging from 1 to 10 days. The solids were identified as ICCs. Liquid assisted grinding was performed with methanol as solvent, while water was utilized for the slurry experiments. Different stoichiometric ratios were employed to check for all the possible cocrystal forms and to determine the most stable forms. The main results are listed in Table 1. Stoichiometric excess of $CaCl_2$ or $MgCl_2$ was never detected in X-ray powder diffraction patterns, as these salts are deliquescent and contribute only to the background.

Table 1. ICCs obtained by reacting etiracetam (ETI) and levetiracetam (LEV) with $CaCl_2$ and $MgCl_2$.

	ICC [method]
LEV:$CaCl_2$ 1:1, 2:1, 4:1	LEV$_2$·$CaCl_2$·$2H_2O$ [LAG, sl, sol]
ETI:$CaCl_2$ 1:1, 2:1, 4:1	ETI$_2$·$CaCl_2$·$2H_2O$ [LAG, sl, sol]
LEV:$MgCl_2$ 1:1, 2:1, 4:1*	LEV$_2$·$MgCl_2$·$2H_2O$ [LAG, sl, sol]
ETI:$MgCl_2$ 1:1	ETI$_2$·$MgCl_2$·$6H_2O$ [LAG, sl, sol] ETI$_4$·$MgCl_2$·$6H_2O$ [sl] ETI$_2$·$MgCl_2$·$2H_2O$ [HSM]
ETI:$MgCl_2$ 2:1	ETI$_4$·$MgCl_2$·$4H_2O$ [LAG] ETI$_4$·$MgCl_2$·$6H_2O$ [sl, sol]
ETI:$MgCl_2$ 4:1	ETI$_4$·$MgCl_2$·$6H_2O$ [LAG, sol]

* no results from solution

LAG = liquid assisted grinding; sl = slurry; sol = evaporation from solution; HSM = hot stage microscopy

Table 1 shows a surprising difference in behavior depending on the nature of the inorganic salt used. The number of accessible forms, the nature of the racemate, the stoichiometry and the hydration of the final ICCs are all markedly dependent on the nature of the salt. For this reason the peculiarities of the interaction of the investigated racetams with each inorganic salt will be discussed in detail, to attempt a rationale for this variety.

Cocrystals of levetiracetam and etiracetam with $CaCl_2$. Cocrystallization of calcium chloride with racemic mixture ETI and LEV appeared to be quite straightforward. In both cases only one crystalline form of ICC was detected, regardless of the solvent or the method applied (Scheme 1). Single crystals for the LEV and ETI ICCs could be obtained both from solution and from the melt, and were characterized as hydrates of formula LEV$_2$·$CaCl_2$·$2H_2O$ and ETI$_2$·$CaCl_2$·$2H_2O$. Regardless of the application of different stoichiometric ratios, we always got the same ICC, along with the excess of unreacted starting material. The racemic and the enantiopure ICCs are quasi-isostructural[31] (Table 2 and Fig. 2) due to the position of the chiral center in ETI molecule not directly involved in the crystal packing, which will be discussed in detail.

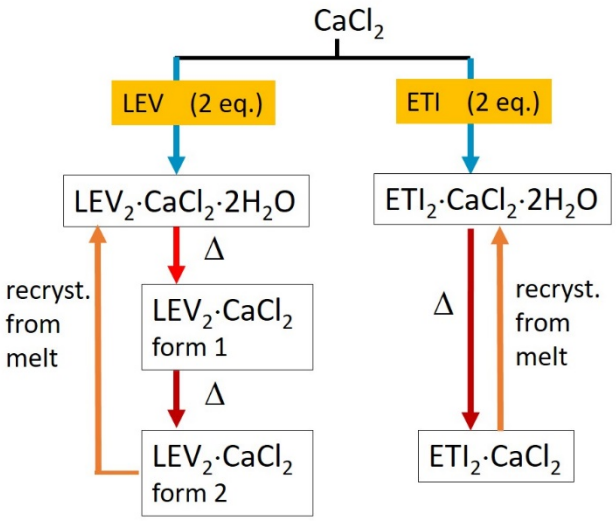

Scheme 1. ICCs of LEV and ETI with $CaCl_2$.

In both hydrated ICCs LEV$_2$·$CaCl_2$·$2H_2O$ and ETI$_2$·$CaCl_2$·$2H_2O$ an octahedral coordination is observed around the metal cation (Fig. 2a), comprising the oxygens of 4 different molecules of LEV (2 oxygens of amide group and two of pyrrolidinone) and two water molecules. Each LEV interacts in turn with a second Ca^{2+} ion through its amide and pyrrolidinone groups, resulting in a 2:1 stoichiometry and a 2D-layered structures (Fig. 2b). Parallel layers (Fig. 2c) are connected to each other via hydrogen bonds between chlorides and amide NH_2 groups or water molecules (Tables S1 and S2). It is noteworthy that the calcium complexation is enantioselective in the racemic crystal of ETI$_2$·$CaCl_2$·$2H_2O$. Fig. 2c right shows how the crystal is composed of distinct chains of R-ETI and S-ETI (LEV), as observed in crystalline LEV$_2$·$CaCl_2$·$2H_2O$. Superposition of the R-ETI layer onto LEV layer reveals that the overall layer conformation is kept and that the

molecules are able to adapt themselves to the local change in chirality (Fig. SI-1). This packing choice is reminiscent of what systematically observed on crystals of the amino acids DL-histidine[23-24] and DL-proline[25] with alkali and alkaline earth halides.

Table 2. Crystal data and details of measurements for the hydrated ICCS of LEV and ETI with $CaCl_2$ and $MgCl_2$.

	$LEV_2{\cdot}CaCl_2{\cdot}2H_2O$	**$ETI_2{\cdot}CaCl_2{\cdot}2H_2O$**	**$LEV_2{\cdot}MgCl_2{\cdot}2H_2O$**	**$ETI_2{\cdot}MgCl_2{\cdot}6H_2O$**	**$ETI_2{\cdot}MgCl_2{\cdot}2H_2O$**	**$ETI_4{\cdot}MgCl_2{\cdot}6H_2O$**
Formula	$(C_8H_{14}N_2O_2)_2 \cdot CaCl_2{\cdot}2H_2O$	$(C_8H_{14}N_2O_2)_2 \cdot CaCl2{\cdot}2H_2O$	$(C_8H_{14}N_2O_2)_2 \cdot MgCl_2{\cdot}2H_2O$	$(C_8H_{14}N_2O_2)_2 \cdot MgCl_2{\cdot}6H_2O$	$(C_8H_{14}N_2O_2)_2 \cdot MgCl_2{\cdot}4H_2O$	$(C_8H_{14}N_2O_2)_4 \cdot MgCl_2{\cdot}6H_2O$
M_r /g mol^{-1}	487.43	487.43	471.66	543.73	471.66	884.17
Crystal system	Monoclinic	Monoclinic	Monoclinic	Triclinic	Monoclinic	Triclinic
Space group	*C*2	*C*2/c	*C*2	*P*-1	*C*2/c	*P*-1
a /Å	14.8240(13)	14.0692(9)	14.0812(5)	8.0745(7)	13.7487(19)	9.0093(8)
b /Å	10.8951(9)	10.8625(5)	10.7596(4)	8.6611(10)	10.5711(11)	10.8861(11)
c /Å	16.3589(16)	17.1740(10)	16.1135(6)	10.4496(12)	17.042(2)	14.1818(14)
α / °	90	90	90	81.505(10)	90	111.917(10)
β / °	108.273(10)	109.330(6)	106.817(4)	80.533(8)	111.873(16)	90.833(8)
γ / °	90	90	90	77.491(9)	90	111.912(9)
V /Å^3	2508.9(4)	2476.7(2)	2336.92(16)	698.93(13)	2298.5(5)	1177.9(2)
Z'	1	0.5	1	0.5	0.5	0.5
Z	4	4	4	1	4	1
d_{calc} /mg.cm^{-3}	1.290	1.307	1.339	1.292	1.363	1.246
μ /mm^{-1}	0.498	0.504	0.343	0.305	0.348	0.216
θ-range /°	3.24-29.18	3.68-29.46	2.93-26.02	3.88-26.28	4.05-19.92	3.64-29.58
Refls measd /unique	6235/4463	5524/ 2871	8200/4319	5610/3188	4209/2032	9537/5423
GoF	1.098	1.076	1.028	0.964	0.949	1.037
R_1 (obsd) [I>2σ(I)]	0.067	0.063	0.038	0.065	0.081	0.069
wR_2 (all)	0.119	0.158	0.1069	0.196	0.263	0.204

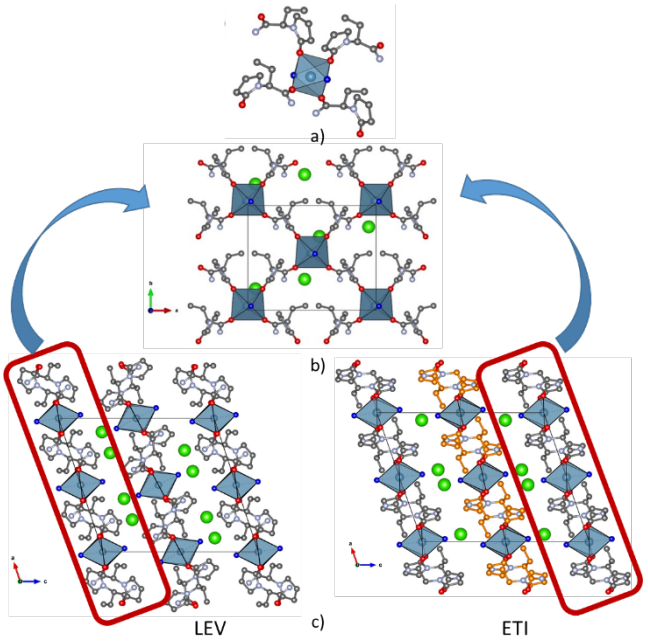

Fig. 2. a) Coordination around the Ca^{2+} cation in crystalline $LEV_2{\cdot}CaCl_2{\cdot}2H_2O$ and $ETI_2{\cdot}CaCl_2{\cdot}2H_2O$. b) A single 2D-layer of Ca^{2+} ions, coordinated water and racetam molecules extending in the *ab*-plane in crystalline $LEV_2{\cdot}CaCl_2{\cdot}2H_2O$ and $ETI_2{\cdot}CaCl_2{\cdot}2H_2O$; c) parallel 2D-layers projected down the b-axis in both ICCs. In addition to the strong coulombic component, hydrogen bonds (not shown for clarity) are at work between the chloride ions and the NH_2 (amide) groups/water molecules. Water oxygens in blue; grey and orange spheres for $ETI_2{\cdot}CaCl_2{\cdot}2H_2O$ refer to racetams with opposite chirality; H_{CH} atoms omitted for clarity.

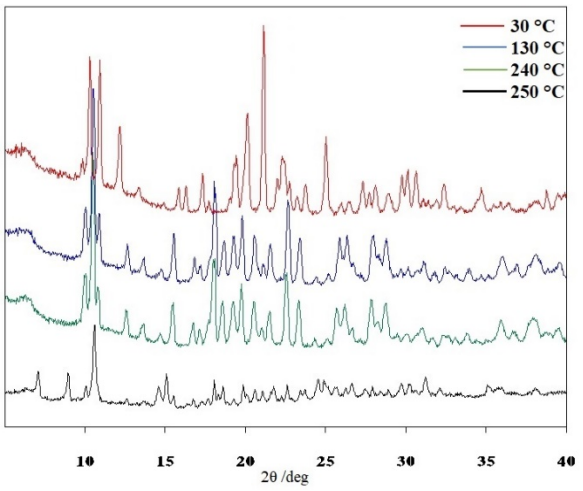

Fig. 3. VT-XRPD for $LEV_2{\cdot}CaCl_2{\cdot}2H_2O$ measured at different temperatures showing the transition to a high temperature form above 240 °C.

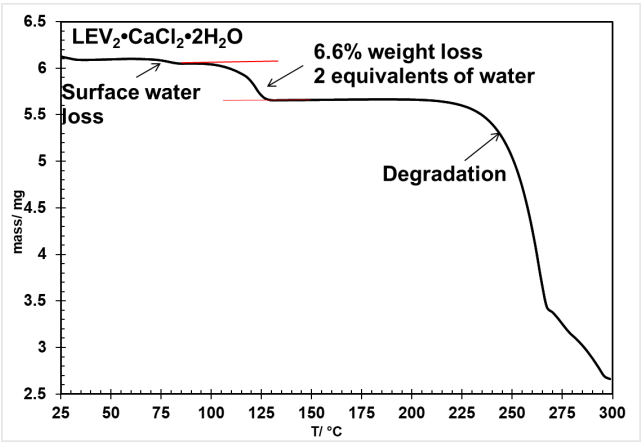

Fig. 4. TGA of $LEV_2{\bullet}CaCl_2{\bullet}2H_2O$

To study the thermal stability of the ICCs, VT-XRPD studies were performed. At room temperature, the XRPD pattern of $LEV_2{\cdot}CaCl_2{\cdot}2H_2O$ corresponds to the simulated pattern obtained from single crystal data. Upon heating $LEV_2{\cdot}CaCl_2{\cdot}2H_2O$ a number of events are observed. The TGA trace shows a steady weight loss (Fig. 4) up to 80 °C, which can easily be attributed to adsorbed surface water, an observable for all ICCs discussed and due to the hygroscopicity of the obtained ICCs. Between 90 °C and 130 °C a loss of 6.6% in weight corresponds to the loss of the 2 equivalents of water of the dihydrate (theoretical weight loss =7.5%), as also confirmed by VT-XRPD (Fig. 3). This anhydrous form remains stable up to 240 °C, temperature at which a transformation to a second anhydrous form occurs, followed by degradation. If the heating is stopped right before degradation occurs, and the sample is cooled back to room temperature, the initial $LEV_2{\cdot}CaCl_2{\cdot}2H_2O$ is again obtained.

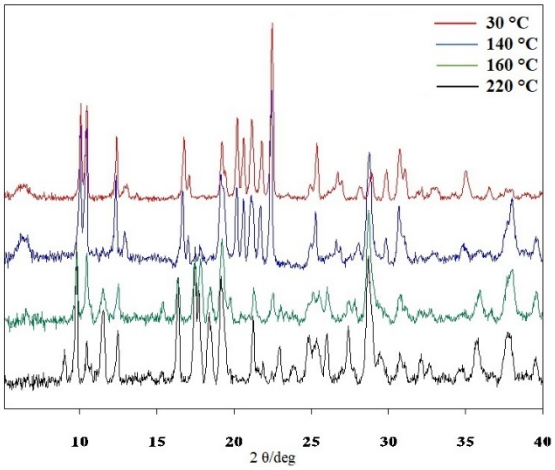

Fig. 5. VT-XRPD for $ETI_2{\cdot}CaCl_2{\cdot}2H_2O$

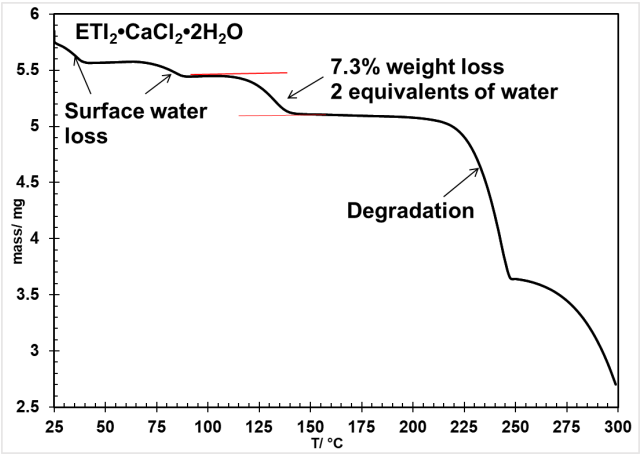

Fig. 6. TGA of $ETI_2{\bullet}CaCl_2{\bullet}2H_2O$

The thermal behavior of $ETI_2{\cdot}CaCl_2{\cdot}2H_2O$ (Fig. 5 and 6) is similar to that of $LEV_2{\cdot}CaCl_2{\cdot}2H_2O$. At room temperature the XRPD pattern of $ETI_2{\cdot}CaCl_2{\cdot}2H_2O$ corresponds to the simulated pattern obtained from single crystal data. Surface water is lost up to 80 °C (when the sample is left for prolonged periods at 80 °C, cooled to 25 °C under nitrogen flow and reheated, one no longer observes the endotherms related to the evaporation of the surface water, Fig. SI-7 and SI-8). The dehydration process starts above 140 °C (Fig. 5), and corresponds to the loss of two water molecules (7.3% aligns with the theoretical loss of 7.5%). The dihydrate of the racemic compound thus has a higher thermal stability compared to that of the enantiopure compound. No further changes in the crystal phase of the anhydrate are observed up to its degradation occurring at 230 °C. If the anhydrate is cooled to room temperature, the initial dihydrate ICC is again obtained.

Cocrystals of levetiracetam with $MgCl_2$. Cocrystallization of LEV with $MgCl_2$ led to the formation of $LEV_2{\cdot}MgCl_2{\cdot}2H_2O$, which is isomorphous with the $CaCl_2$ analogue (Table 2). As in the case of the ICC with $CaCl_2$, only one stoichiometry was observed, irrespective of the starting stoichiometric ratio, solvent used and method

employed to obtain the cocrystals (Scheme 2). The thermal behavior (Fig. 7 and 8) parallels the one observed for $LEV_2{\cdot}CaCl_2{\cdot}2H_2O$, with surface water removal up to 100 °C and a single dehydration process observed at ca. 150 °C (experimental weight loss by TGA=8.6% ; theoretical weight loss =7.6%); the anhydrate phase thus obtained remains stable up to 240 °C. If the dehydration process is followed via HSM, melting is observed for the anhydrous phase at 240 °C, and recrystallization of the melt under ambient conditions yields the dihydrated ICC $LEV_2{\cdot}MgCl_2{\cdot}2H_2O$.

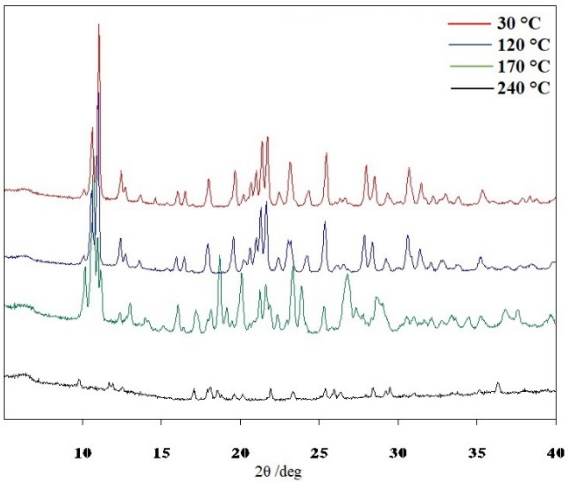

Fig. 7. VT-XRPD for $LEV_2{\cdot}MgCl_2{\cdot}2H_2O$

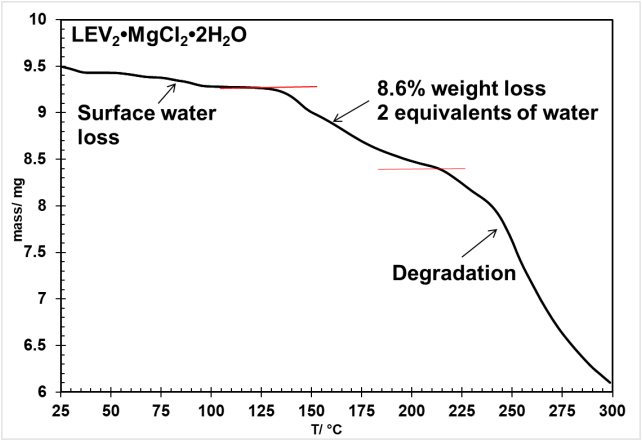

Fig. 8. TGA of $LEV_2{\cdot}MgCl_2{\cdot}2H_2O$

Cocrystals of etiracetam with $MgCl_2$. Cocrystallization of racemic mixture ETI with $MgCl_2$ leads to a more complex solid state landscape, with the outcome being dependent on reaction and stoichiometric conditions (scheme 2). Different stoichiometries are obtained, namely $ETI_2{\cdot}MgCl_2{\cdot}6H_2O$ (2:1 system) and $ETI_4{\cdot}MgCl_2{\cdot}6H_2O$ (4:1 system), and the cocrystals are hexahydrates, contrary to the dihydrates observed for all other cases. Thermal dehydration processes will lead to intermediate hydrate phases, as will be discussed below.

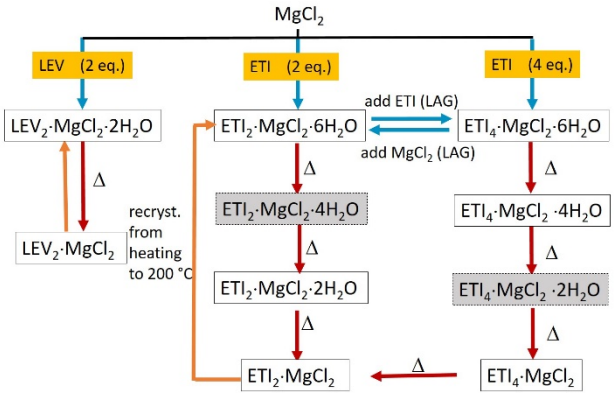

Scheme 2. ICCs of LEV and ETI with $MgCl_2$. Grey boxes are put when the forms were only observed in VT XRPD. There is an interconversion between $ETI_2{\cdot}MgCl_2{\cdot}6H_2O$ and $ETI_4{\cdot}MgCl_2{\cdot}6H_2O$ using LAG and by addition of the appropriate amount of reactant.

2:1 system - the ICC $ETI_2{\cdot}MgCl_2{\cdot}nH_2O$ (n = 2, 6). Reaction of ETI with $MgCl_2$ in 1:1 stoichiometry, with the intent of obtaining $ETI_2{\cdot}MgCl_2{\cdot}2H_2O$, i.e. the $CaCl_2$ analogue, yielded an oil, which in a matter of a few days crystallized into the hexa-hydrated ICC of formula $ETI_2{\cdot}MgCl_2{\cdot}6H_2O$ (Fig. 9). The Mg^{2+} cation is hexacoordinated by two pyrrolidinone oxygens - belonging to ETI R and S enantiomers - and by four water molecules, thus forming a 0D complex instead of the 1D chains encountered in the previously discussed ICCs. The amido groups are hydrogen bonded to the chloride anions and to water molecules via the $-NH_2$ and -C=O moieties, respectively (Table S4).

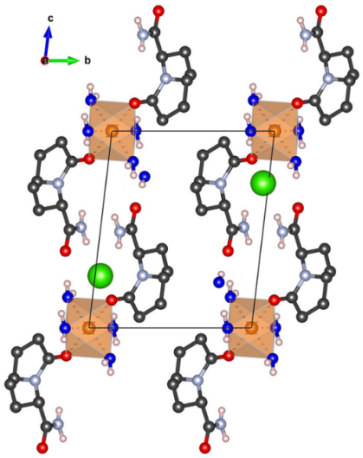

Fig. 9. 0D-complexes in crystalline ICCs $Eti_2{\cdot}MgCl_2{\cdot}6H_2O$. Water molecules marked in blue; H_{CH} atoms omitted for clarity.

Upon heating, three subsequent transitions occur. A first transition occurs at around 70 °C, a second at 100 °C and a third at 130 °C. TGA trace and VT-XRPD patterns (Fig. 10 and 11) confirm that each step corresponds to the loss of two water molecules (21.6% total weight loss,

theoretical loss of 6 water molecules = 19.9%). Degradation occurs starting from 250 °C. Based on this analysis, it can be inferred that a hexa-hydrate, a tetra-hydrate, a di-hydrate and an anhydrate phase to exist for the 2:1 cocrystal.

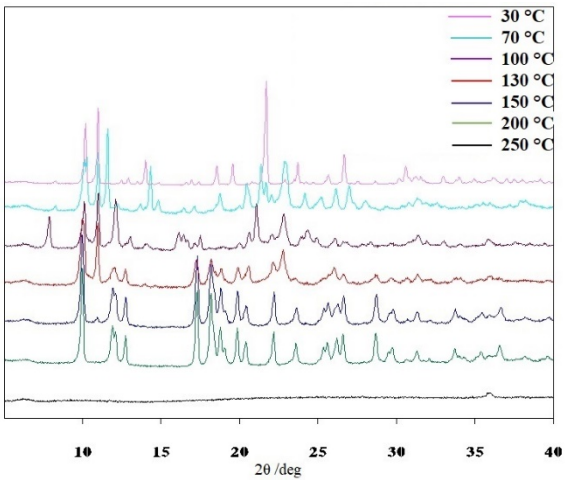

Fig. 10. VT XRPD for $Eti_2{\cdot}MgCl_2{\cdot}6H_2O$.

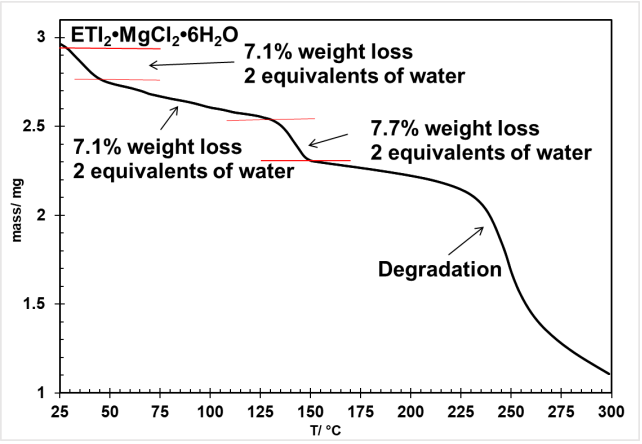

Fig. 11. TGA of $ETI_2{\bullet}MgCl_2{\bullet}6H_2O$

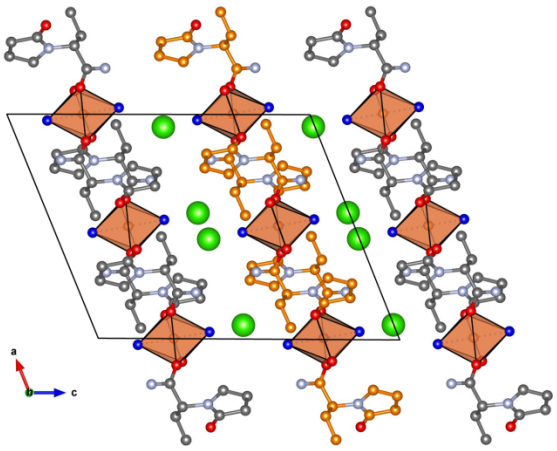

Fig. 12. $ETI_2{\cdot}MgCl_2{\cdot}2H_2O$. View down the crystallographic *b*-axis.

In addition to the hexahydrate $ETI_2{\cdot}MgCl_2{\cdot}6H_2O$ ICC, single crystals of the di-hydrated $ETI_2{\cdot}MgCl_2{\cdot}2H_2O$ could also be obtained, as the product of recrystallization of $ETI_2{\cdot}MgCl_2{\cdot}6H_2O$ from the melt in a Hot Stage Microscopy experiment, in a similar approach to the one employed to produce single crystals of $LEV_2{\cdot}CaCl_2{\cdot}2H_2O$ from the melt (SI-Hot Stage Microscopy experiment). The obtained crystals were analyzed and shown to be isomorphous with the calcium analogue $ETI_2{\cdot}CaCl_2{\cdot}2H_2O$ (Fig. 12). On the basis of the crystal structure of the hexahydrate and the dihydrate, we can conclude that the three successive water losses of the hexahydrate upon heating correspond to the loss of the water molecules not bound to the Mg^{2+} cation, followed by the loss of two of the four Mg^{2+} bound water molecules, and finally to the last two Mg^{2+} bound water molecules of the dihydrate.

4:1 system - the ICCs $ETI_4{\cdot}MgCl_2{\cdot}nH_2O$ (n=4,6) Cocrystallization from water of ETI with $MgCl_2$, this time in a 4:1 stoichiometric ratio, yielded the hexahydrate ICC $ETI_4{\cdot}MgCl_2{\cdot}6H_2O$ (Fig 13).

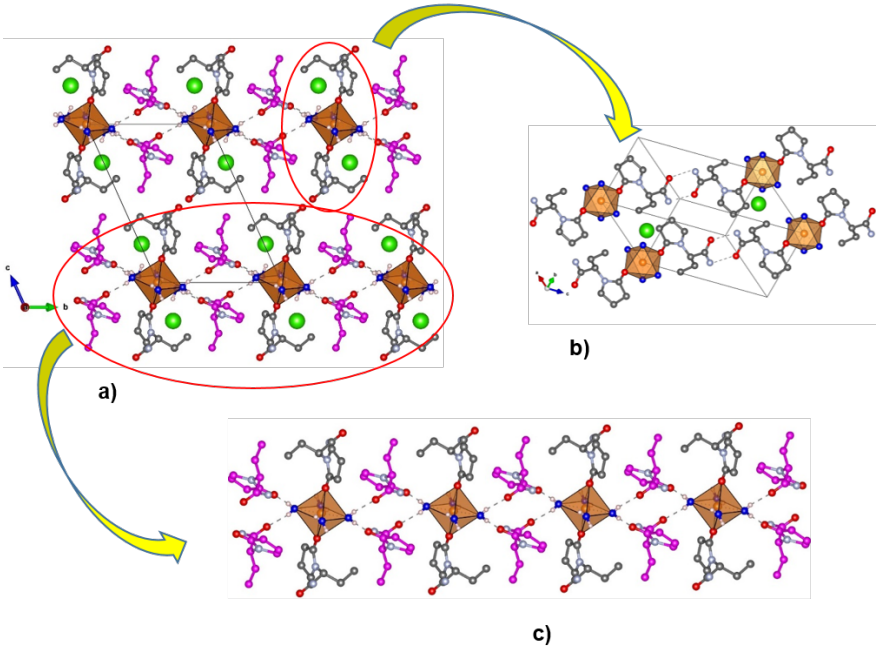

Fig. 13. $ETI_4{\cdot}MgCl_2{\cdot}6H_2O$. a) View along crystallographic a-axis. b) CO···NH hydrogen bonds among ETI molecules involved in the magnesium coordination. c) 1D chains by ETI molecules uncoordinated to Mg^{2+} cations. Water molecules are marked in blue, Mg^{2+} cations are marked in orange, the carbon atoms of ETI molecules which are not involved into coordination with Mg^{2+} are marked in violet, hydrogens are omitted for clarity and dash lines are hydrogen bonds.

As for the 2:1 cocrystal, an octahedral coordination is observed around the Mg^{2+} cation with 2 molecules of ETI (both R and S enantiomers) and 4 water molecules forming a 0D complex. In the 4:1 cocrystal $ETI_4{\cdot}MgCl_2{\cdot}6H_2O$ only the oxygens of pyrrolidinone are involved in the coordination with Mg^{2+}, whereas the amide groups of ETI form CO···NH hydrogen bonds (Fig. 13b). One peculiarity of this structure is the presence of layers of ETI (R and S enantiomers) uncoordinated to Mg^{2+} cations. These ETI molecules form 1D chains *via* hydrogen bonds with water molecules coordinated to Mg^{2+} (Fig. 13c). These chains are held together via hydrogen bonds between amide groups and via NH_2---Cl^- and HOH---Cl^- hydrogen bonds (Table S6). The $ETI_4{\cdot}MgCl_2{\cdot}6H_2O$ ICC could thus be seen as a "cocrystal" of $ETI_2{\cdot}MgCl_2{\cdot}6H_2O$ and ETI. Grinding of $ETI_4{\cdot}MgCl_2{\cdot}6H_2O$ with one equivalent of MgCl2, indeed, leads to $ETI_2{\cdot}MgCl_2{\cdot}6H_2O$, whereas grinding of this latter with 2 equivalents of ETI leads to $ETI_4{\cdot}MgCl_2{\cdot}6H_2O$.

VT-XRPD patterns and TGA trace (Fig. 14 and 15) show the loss of two water molecules from $ETI_4{\cdot}MgCl_2{\cdot}6H_2O$ between 80 °C and 100 °C (4.3% weight loss, theoretical w%=4.1). Four further H_2O molecules are lost between 120 °C and 160 °C (7.8% weight loss, theoretical w%=8.2). The weight loss between 160-200 °C is caused by the loss of 2 equivalents of ETI, which are not coordinated to the Mg^{2+} cation (41.4% weight loss, theoretical w%=38.5). The resulting $ETI_2{\cdot}MgCl_2$ anhydrate form remains stable up to 245 °C.

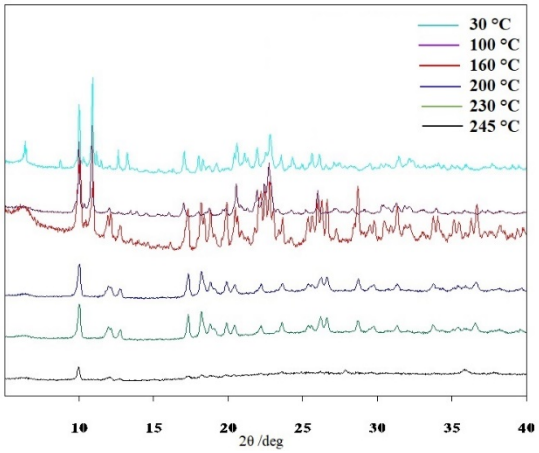

Fig. 14. VT XRPD for $Eti_4{\cdot}MgCl_2{\cdot}6H_2O$.

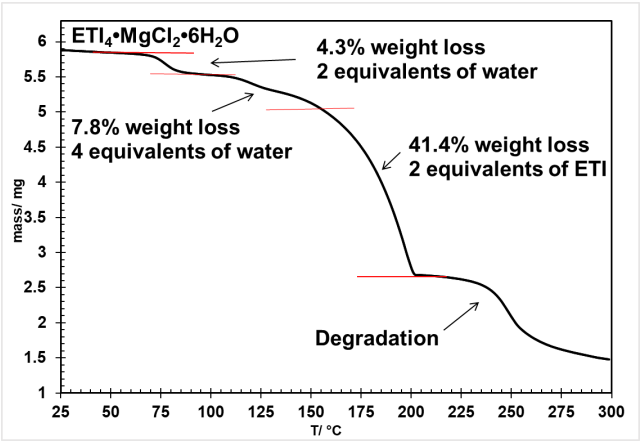

Fig. 15. TGA of ETI_4•$MgCl_2$•$6H_2O$

Surprisingly, ETI_4·$MgCl_2$·$4H_2O$ was formed by MeOH LAG of ETI with $MgCl_2$ using a 2:1 stoichiometry, which was shown by a comparison of the XRPD patterns of the ground phase and the pattern of ETI_4·$MgCl_2$·$6H_2O$ heated to 100°C (temperature at which 2 water molecules are lost) (Fig. 16). The thermal behavior above 100°C of this ground phase (Fig. SI-12) is found identical to that of ETI_4·$MgCl_2$·$6H_2O$.

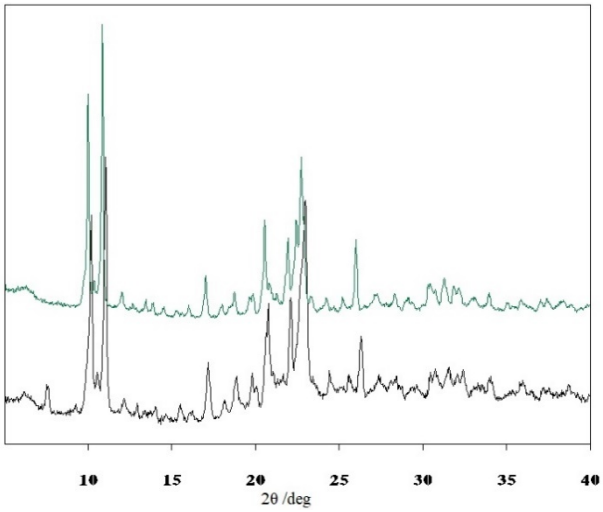

Fig. 16. XRPD patterns of Eti_4·$MgCl_2$·$6H_2O$ heated to 100°C (cyan line) and the MeOH LAG ground sample (black line).

Stability tests for ETI ICCs with $MgCl_2$. As shown above, the combination of ETI and $MgCl_2$ leads to multiple hydrate forms. Slurry experiments (Table 1) performed at 25 °C show the hexahydrate forms ETI_2·$MgCl_2$·$6H_2O$ and ETI_4·$MgCl_2$·$6H_2O$ to be the most stable phases in water at 25°C.

CONCLUSIONS

The interaction of enantiopure LEV and racemic ETI with the pharmaceutically acceptable inorganic salts $CaCl_2$ and $MgCl_2$ was investigated. It was found that both ETI and LEV formed crystalline dihydrates with $CaCl_2$, namely ETI_2·$CaCl_2$·$2H_2O$ and LEV_2·$CaCl_2$·$2H_2O$ which possess similar structures and lead to anhydrates at temperatures above 120°C.

The interaction with $MgCl_2$ led to a complex solid state landscape. While the enantiopure LEV produced only one ICC isostructural with LEV_2·$CaCl_2$·$2H_2O$, the cocrystallization with ETI led to the formation of multiple crystalline phases. The crystallization from slurry and solutions typically led to formation of stoichiometrically diverse ETI_2·$MgCl_2$·$6H_2O$ or ETI_4·$MgCl_2$·$6H_2O$ cocrystals. The 4:1 cocrystal can be seen as a cocrystal between the 2:1 phase and ETI, with the interconversion illustrated by grinding experiments. Both hexahydrate phases lead to tetra-, dihydrate and anhydrate phases upon heating. It is noteworthy that ETI_2·$MgCl_2$·$2H_2O$, which is isostructural with ETI_2·$CaCl_2$·$2H_2O$, shows the same type of homochiral preference for etiracetam molecules of the same chirality (S-ETI and R-ETI) upon complexation with the Ca^{2+} cations.

All cocrystals showed a significant increase in the thermal stability of both LEV and ETI in the ICCs with respect to the parent organic systems. All ICCs underwent dehydration and showed thermal stability up to 240-260 °C.

ASSOCIATED CONTENT

Supporting Information. Supporting information files are available free of charge via the Internet at http://pubs.acs.org. Additional experimental data, superimposition information, details of hydrogen bonds, Experimental XRPD and DSC curves (PDF).

CCDC 1894095-1894100 contain the supplementary crystallographic data for this paper. The data can be obtained free of charge from The Cambridge Crystallographic Data Centre via www.ccdc.cam.ac.uk/structures. (or from the Cambridge Crystallographic Data Centre, 12 Union Road, Cambridge CB21EZ, UK; fax: (+44)1223-336-033; or e-mail: deposit@ccdc.cam.ac.uk).

AUTHOR INFORMATION

Corresponding Author

* E-mail: tom.leyssens@uclouvain.be; fabrizia.grepioni@unibo.it.

ORCID:

Lixing Song: 0000-0003-4874-3551

ACKNOWLEDGMENT

This work was supported by a STSM Grant from COST Action CM1402 Crystallize. Lixing Song would like to thank the China Scholarship Council (CSC) for financial support.

REFERENCES:

1. Scheuer, M. L.; Pedley, T. A. The Evaluation and Treatment of Seizures. *N. Engl. J. Med.* **1990,** *323*, 1468-1474.
2. Brodie, M. J.; Shorvon, S. D.; Canger, R.; Halász, P.; Johannessen, S.; Thompson, P.; Wieser, H. G.; Wolf, P. Commission on European Affairs: Appropriate Standards of Epilepsy Care Across Europe. *Epilepsia* **1997,** *38*, 1245-1250.
3. Hovinga Collin, A. Levetiracetam: A Novel Antiepileptic Drug. *Pharmacotherapy* **2012,** *21*, 1375-1388.
4. Gouliaev, A. H.; Senning, A. Piracetam and other structurally related nootropics. *Brain Res. Rev.* **1994,** *19*, 180-222.
5. Braga, D.; Grepioni, F.; Maini, L.; Prosperi, S.; Gobetto, R.; Chierotti, M. R. From unexpected reactions to a new family of ionic co-crystals: the case of barbituric acid with alkali bromides and caesium iodide. *Chem. Commun.* **2010,** *46*, 7715-7717.
6. Smith, A. J.; Kim, S.-H.; Duggirala, N. K.; Jin, J.; Wojtas, L.; Ehrhart, J.; Giunta, B.; Tan, J.; Zaworotko, M. J.; Shytle, R. D. Improving Lithium Therapeutics by Crystal

Engineering of Novel Ionic Cocrystals. *Mol. Pharmaceutics* **2013,** *10*, 4728-4738.
7. Delori, A.; Galek, P. T. A.; Pidcock, E.; Patni, M.; Jones, W. Knowledge-based hydrogen bond prediction and the synthesis of salts and cocrystals of the anti-malarial drug pyrimethamine with various drug and GRAS molecules. *CrystEngComm* **2013,** *15*, 2916-2928.
8. Kelley, S. P.; Narita, A.; Holbrey, J. D.; Green, K. D.; Reichert, W. M.; Rogers, R. D. Understanding the Effects of Ionicity in Salts, Solvates, Co-Crystals, Ionic Co-Crystals, and Ionic Liquids, Rather than Nomenclature, Is Critical to Understanding Their Behavior. *Cryst. Growth Des.* **2013,** *13*, 965-975.
9. Butterhof, C.; Barwinkel, K.; Senker, J.; Breu, J. Polymorphism in co-crystals: a metastable form of the ionic co-crystal 2 HBz[middle dot]1 NaBz crystallised by flash evaporation. *CrystEngComm* **2012,** *14*, 6744-6749.
10. Braga, D.; Grepioni, F.; Shemchuk, O. Organic–inorganic ionic co-crystals: a new class of multipurpose compounds. *CrystEngComm* **2018,** *20*, 2212-2220.
11. Shemchuk, O.; Braga, D.; Maini, L.; Grepioni, F. Anhydrous ionic co-crystals of cyanuric acid with LiCl and NaCl. *CrystEngComm* **2017,** *19*, 1366-1369.
12. Braga, D.; Grepioni, F.; Maini, L.; Capucci, D.; Nanna, S.; Wouters, J.; Aerts, L.; Quere, L. Combining piracetam and lithium salts: ionic co-crystals and co-drugs? *Chem. Commun.* **2012,** *48*, 8219-8221.
13. Oertling, H. Interactions of alkali- and alkaline earth-halides with carbohydrates in the crystalline state - the overlooked salt and sugar cocrystals. *CrystEngComm* **2016,** *18*, 1676-1692.
14. Braga, D.; Grepioni, F.; Lampronti, G. I.; Maini, L.; Turrina, A. Ionic Co-crystals of Organic Molecules with Metal Halides: A New Prospect in the Solid Formulation of Active Pharmaceutical Ingredients. *Cryst. Growth Des.* **2011,** *11*, 5621-5627.
15. Buist, A. R.; Kennedy, A. R. Ionic Cocrystals of Pharmaceutical Compounds: Sodium Complexes of Carbamazepine. *Cryst. Growth Des.* **2014,** *14*, 6508-6513.
16. Honer, K.; Kalfaoglu, E.; Pico, C.; McCann, J.; Baltrusaitis, J. Mechanosynthesis of Magnesium and Calcium Salt–Urea Ionic Cocrystal Fertilizer Materials for Improved Nitrogen Management. *ACS Sustainable Chem. Eng.* **2017,** *5*, 8546-8550.
17. Wouters, J.; Grepioni, F.; Braga, D.; Kaminski, R. M.; Rome, S.; Aerts, L.; Quéré, L. Novel pharmaceutical compositions through co-crystallization of racetams and Li+ salts. *CrystEngComm* **2013,** *15*, 8898.
18. Duggirala, N. K.; Smith, A. J.; Wojtas, Ł.; Shytle, R. D.; Zaworotko, M. J. Physical Stability Enhancement and Pharmacokinetics of a Lithium Ionic Cocrystal with Glucose. *Cryst. Growth Des.* **2014,** *14*, 6135-6142.
19. Leyssens, T.; Horst, J. t., Solution Co-crystallization and its applications. In *Multi-component Crystals: Synthesis, Concepts, Function*, De Gruyter: 2017; 205-236.
20. Regulatory Classification of Pharmaceutical Co-crystals: Guidance for Industry. *Administration, F. a. D.* **2018.**
21. Springuel, G.; Leyssens, T. Innovative Chiral Resolution Using Enantiospecific Co-Crystallization in Solution. *Cryst. Growth Des.* **2012,** *12*, 3374-3378.
22. George, F.; Norberg, B.; Robeyns, K.; Wouters, J.; Leyssens, T. Peculiar Case of Levetiracetam and Etiracetam α-Ketoglutaric Acid Cocrystals: Obtaining a Stable Conglomerate of Etiracetam. *Cryst. Growth Des.* **2016,** *16*, 5273-5282.
23. Braga, D.; Degli Esposti, L.; Rubini, K.; Shemchuk, O.; Grepioni, F. Ionic Cocrystals of Racemic and Enantiopure Histidine: An Intriguing Case of Homochiral Preference. *Cryst. Growth Des.* **2016,** *16*, 7263-7270.
24. Shemchuk, O.; Degli Esposti, L.; Grepioni, F.; Braga, D. Ionic co-crystals of enantiopure and racemic histidine with calcium halides. *CrystEngComm* **2017,** *19*, 6267-6273
25. Shemchuk, O.; Tsenkova, B. K.; Braga, D.; Duarte, M. T.; Andre, V.; Grepioni, F. Ionic Co-Crystal Formation as a Path Towards Chiral Resolution in the Solid State. *Chem. - Eur. J.* **2018,** *24*, 12564-12573.
26. Shemchuk, O.; Song, L.; Robeyns, K.; Braga, D.; Grepioni, F.; Leyssens, T. Solid-state chiral resolution mediated by stoichiometry: crystallizing etiracetam with ZnCl2. *Chem. Commun.* **2018,** *54*, 10890-10892.
27. Budavari, S.; O'Neil, M.; Smith, A.; Heckelman, P. The Merck index : an encyclopedia of chemicals, drugs, and biologicals. Whitehouse Station, N.J Merck 2001: 2001.
28. Grepioni, F.; Wouters, J.; Braga, D.; Nanna, S.; Fours, B.; Coquerel, G.; Longfils, G.; Rome, S.; Aerts, L.; Quere, L. Ionic co-crystals of racetams: solid-state properties enhancement of neutral active pharmaceutical ingredients via addition of Mg2+ and Ca2+ chlorides. *CrystEngComm* **2014,** *16*, 5887-5896.
29. Sheldrick, G. M. Crystal structure refinement with SHELXL. *Acta Crystallogr., Sect. C: Struct. Chem.* **2015,** *71*, 3-8.
30. Braga, D.; Maini, L.; Grepioni, F. Mechanochemical preparation of co-crystals. *Chem. Soc. Rev.* **2013,** *42*, 7638-7648.
31. Kalman, A.; Parkanyi, L.; Argay, G. Classification of the Isostructurality of Organic Molecules in the Crystalline State. *Acta Crystallogr., Sect. B: Struct. Sci.* **1993,** *49*, 1039-1049.